# Robust detection of hidden material damages using low-cost external sensors and Machine Learning

**Stefan Bosse[1], Dirk Lehmhus[2]**

[1]University of Bremen, Dept. of Mathematics and Computer Science
[2]Fraunhofer IFAM, Bremen

**Abstract:** Machine Learning (ML) techniques are widely used in Structural Health Monitoring (SHM) and Non-destructive Testing (NDT), but the learning process, the learned models. and the prediction consistency are poorly understood. This work investigates and compares a wide range of ML models and algorithms for the detection of hidden damages in materials monitored using low-cost strain sensors. The investigation is performed using a multi-domain simulator imposing a tight coupling of physical and sensor network simulation in the real-time scale. The device under test is approximated by using a mass-spring network and a multi-body physics solver.

## I. Introduction

Non-destructive diagnostics and prediction of damages is still a challenge challenge even in conventional monolithic materials. New materials and hybrid materials, e.g., fiber-metal laminates, are subject to hidden damages without externally visible change of the material. Well established measuring techniques are ultra-sonic monitoring and computer tomography using x-rays. Both techniques suffer from their high instrumental effort and difficulties in diagnostic robustness. External monitoring of internal damages of such materials and structures with simple and low-cost external sensors, e.g., strain-gauge sensors, under run-time conditions is of high interest. But there is a significant gap between knowledge and understanding of damage models and the interpretation of sensor data. Machine Learning (ML) is a promising method to derive sensor-damage relation models based on training data. In [1], artificial neural networks with hidden layers were applied to ultrasonic wave signals to predict structural damages. Although "Deep learning" is attractive and en vogue, it requires commonly a high amount of training data and learning time (high computational costs). The investigation of the suitability of and the identification of alternative approaches to Deep learning with respect to efficiency is addressed in this work.

In this work, a multi-domain simulation study is presented comparing and evaluating different ML algorithms and models, i.e., decision trees (classical *C45*, advanced *ICE*), artificial neural networks (single and multi-layer perceptrons SLP/MLP), and support

vector machines (*SVM*). A simple plate is used as a Device under Test (DUT), which is modelled using a simple physical mass-spring network model (MSN), finally simulated (computed) by a multi-body physics engine. The physical computation of the DUT under varying load situations in real-time is directly performed by the simulator combined with an agent-based simulation of signal processing in a Distributed Sensor Network (DSN). Data processing and learning is performed by a collection of agents implementing centralised and distributed agent-based learning [2].

The signals of artificial strain-gauge sensors placed on the top side of the DUT surface are computed directly from the MSN and are used to predict hidden damages (holes, inhomogeneities, and impurities) by applying ML to unreliable sensor data. Monte Carlo simulation is used to introduce noise and sensor failures. There are some surprising results concerning robustness and usability of different ML algorithms showing that Deep Learning is not always suitable!

The simulator (SEJAM2) combining physical and computational simulation can be used as a generic tool for investigation of ML, sensing, sensor design, and distributed data processing. The entire simulation can be controlled by the user via a chat dialogue controlled by an avatar agent. This feature enables the usage of the simulator for educational purposes, too.

There are three major scientific questions addressed in this work: (1) The suitability and accuracy of mass-spring models, especially for modelling of damages in materials and the generation of suitable sensor signals; (2) The suitability of ML for hidden damage detection using noisy and unreliable low-cost sensors and (3) the comparison of different ML models and algorithms with respect to their prediction accuracy, learning time, and model data size.

## II. Modelling and Simulation

Commonly, the Finite Element Method (FEM) is used to simulate the mechanical behavior of engineering structures. This numerical approach for, among others, solving continuum mechanics problems subdivides the component under scrutiny into small, finite elements (hence the name), solves the partial differential equations describing the respective problem numerically for specific points within these sub-domains and assembles the results to a global solution via local approximation functions which match the functional values obtained for the aforementioned Gauss points and meet certain continuity conditions enforced at transitions between elements. The method as such is accepted and used so widely that it is almost beyond any need for description, much less justification.

However, FEM methods do have disadvantages which tend not to matter in normal engineering analysis, but suddenly become relevant for the investigations – and applications – behind the present study. Most prominent among these drawbacks is the fact that FEM methods suffer from high computational costs. Typically, the computational effort scales linearly with the number of elements, nodes and degrees of freedom (DOF) in the case of static problems, as has e. g. been demonstrated by Miersch et al.

[3].

However, the prerequisite is that sufficient computational resources are available to solve the problem without decomposition of the matrices. If this is not the case, scaling laws will change significantly for the worse. Besides, there is a major difference between static and dynamic simulations, which is based on the fact that the latter are usually performed according to a semi-static principle: Either automatically or by the user, an initial time step is selected which subdivides the time span to be covered into several individual stages, for which static simulations are performed. Even though the length of the time step is typically adjusted during the calculations if stable solutions can be achieved for larger intervals to limit the computational effort, this typically implies an extended effort and thus duration of dynamic as opposed to static calculations. The impact of this general observation on the present study is twofold. It implies that the FEM method would not be suitable to run on a system which will necessarily have limited computational power as well as energy resources and will thus need to economize on computational effort.

Besides, it underlines that an FEM approach, specifically under the aforementioned boundary conditions, is not the optimum choice when real-time solutions are aspired to. For such simulations and evaluation of sensor networks close to the real world, a faster methodology is required, even if this should come at the cost of some levels of accuracy.

There are, however, studies on real-time FEM, but in these, the systems consider tend to be of very low complexity, sometimes with DOF numbers well below 100 [4]. At the same time, alternatives like reduced order modelling techniques cannot be applied, as they base simplification of the original model on special characteristics of the same, while the problem we address in the present work involves damage and thus change of the original system.

For the above reasons, we have chosen a multi-body system approach to represent the material of the structure under study. Multi-body physics are thus generally introduced below.

In the next sub-section, the basic concepts of multi-body physics is introduced as an alternative method for modelling and simulating mechanical structures in real-time order.

### II.1 Multi-body Physics

In its most simple case, multi-body simulation deals with kinematic problems: Rigid bodies are assumed to be linked by various types of joints, which differ in their degrees of freedom and thus constrain the respective system's allowable movements. What is analyzed is motion alone – forces are not accounted for. Multi-body System Dynamics (MBSD) adds the force component. Now the rigid bodies can be linked via various types of interactions. These include e. g. friction forces, but can also simulate materials' characteristics.

For example, it is possible to connect the rigid bodies via spring- (representing material stiffness), damper- (representing time-dependent, viscous behavior) or friction-type (representing ideal plasticity) elements, or combinations of these. In this sense, e.g., viscoelastic properties as seen in many polymers are constructed by parallel arrangement of spring and damper elements, whereas elastoplastic behavior is represented by serial connection of a spring and a friction element.

Naturally, the quality of this type of modelling when describing materials rather than structures does depend on granularity, i. e. on the size of the connected, rigid elements – in fact, in most problems in which multi-body simulations are practically applied, the scale is macroscopic:Examples include vehicle dynamics as well as crash simulations in the automotive (see [5] and [6]), including also bio-mechanical studies [7], or simulations of robotic systems [8].

Several works providing a broad overview of the field both in terms of methods and applications have been published in recent years, e.g., in [9], [5], and [10].

In the current case, though not yet realized in the work we present here, the perspective is towards the microscopic, and to materials rather than structures. For this purpose, we have built up a 3D network of mass elements connected by springs in the manner explained in Fig. 6. In our approach, this network reflects the behavior of the material, and future evolutions will be increased in resolution.

While this approach may seem unusual for MBSD simulation, it does bear some similarities to some notions behind mesh-free simulation methods like Smoothed Particle Hydrodynamics (SPH), Discrete Element Method (DEM) or Material Point Methods (MPM), which also represent materials on a particle basis and through interactions between these particles ([11] and [12]).

*Mass-Spring Systems*

A mechanical structure is modelled with a Graph $St$=<$\mathbf{M}$,$\mathbf{Sp}$>, where $\mathbf{M}$ is a set of mass nodes with a specific mass $m_i$, and $\mathbf{Sp}$ is a set of spring-damper edges connecting mass nodes.

$$St(P) = \langle \mathbf{M(P)}, \mathbf{Sp(P)} \rangle$$

$$\mathbf{M} = \begin{bmatrix} m_1 & \cdots & m_j \\ \vdots & \ddots & \vdots \\ m_i & \cdots & m_n \end{bmatrix}, \mathbf{Sp} = \begin{bmatrix} sp_1 & \cdots & sp_l \\ \vdots & \ddots & \vdots \\ sp_k & \cdots & sp_m \end{bmatrix} \tag{1}$$

Each node $m_i$ has spring connections that are associated to this node pointing to up to seven neighbouring nodes (in three dimensions). details can be found in [14].

The general MSN model graph $St(P)$ is paremeterised by a set of parameters defining the node mass $mm_i$, the spring stiffness constant $sk_j$, and optionally a damper constant $sd_j$. The choice of the parameters, which can be applied to all masses and springs of the network, or individually to domains of nodes and edges, is crucial for the mapping of real physical material behaviour on the physical simulation model described in the next section.

In this work, the node masses and spring constants were chosen to characterise a linear elastic material, typically a purely elastic elastomer.

### II.2 Multi-domain Simulation

1. Multi-body physics (MBP) using the *CANNON* physics engine [13]

2. Multi-agent systems and sensor networks using the *JAM* agent platform

The CANNON physics engine is a constraint based multi-body solver that uses an iterative Gauss-Seidel solver to solve constraints and the SPOOK stepper.

The software architecture of the multi-domain simulator *SEJAM2* is shown in Fig. 1 and 2. The entire simulator is programmed in JavaScript and processed by node-webkit (embedding the V8 JavaScript high-performance engine). Details can be found in [14] and [15].

As already stated in the introductory section, the MBP simulation is faster than classical FEM simulation by several orders of magnitude. E.g., the simulation of a physical structure consisting of about 330 mass nodes and 2500 springs requires about 50 μs for one update computation of the structure (one physical simulation step, calculation of all mass displacements, forces, and spring forces), using a typical mid-range computer and the JavaScript (JS) V8 engine benchmarking at 22000k C dhrystones/s and 6600k JS/V8 dhrystones/s, respectively.

Computational complexity and concrete computation times for FEM depend on algorithms, used equation solvers, and the complexity/size of the FEM graph (i.e., the number of elements, basically). In [4], the FEM computation of a simple model using a 1D model with only 11 elements was evaluated for a micro-controller with an Arm Cortex 4 core (at 180MHz clock frequency). The computation time for one static computation (terminating in a stable state) was about one second. Assuming 5000k C-dhrystones/s/GHz for the used machine, this scales to 50ms on the mid-range desktop computer (1000 times slower) considered before, finally scaled linearly with respect to the number of elements (2500/11) it would require about 10s (or even more). The simulation of the dynamic behaviour investigated in this work requires semi-static step-wise FEM simulation accumulating the simulation times for each step. A typical dynamic simulation run requires about 1000 steps! In [3], investigation of FEM computation times were made with a 3D model showing a more or less linear dependency of the computation time on the number of elements. A structure with about 2000 elements required a computation time of approximately 15 seconds.

The data processing part is performed by agents executed by the JavaScript Agent Machine (*JAM*). A physical *JAM* node supports a world consisting of virtual (logical) nodes (*vJAM*), which are used to compose the artificial sensor network in the simulation. I.e., each sensor node in the simulation world is represented by a *vJAM* instance. Agents perform sensor sampling, sensor processing, aggregation, and learning (either centralised by one learning instance or decentralised by multiple learning instances).
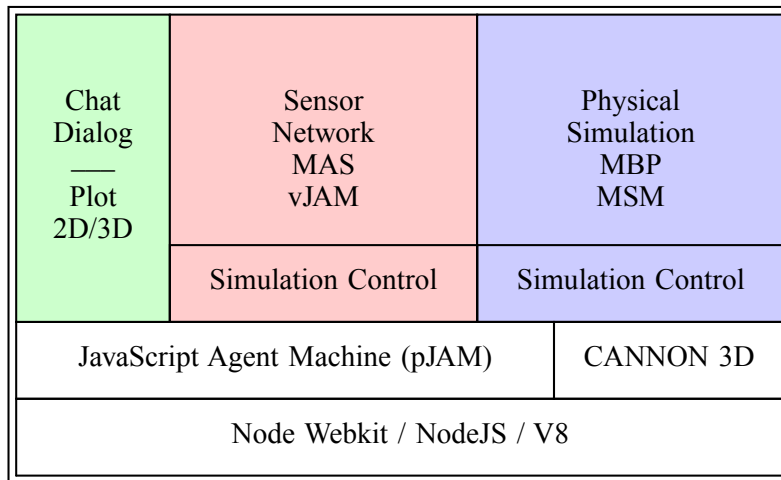
| Chat Dialog —— Plot 2D/3D | Sensor Network MAS vJAM | Physical Simulation MBP MSM |
|---|---|---|
| | Simulation Control | Simulation Control |
| JavaScript Agent Machine (pJAM) | | CANNON 3D |
| Node Webkit / NodeJS / V8 | | |

*Figure 1. Architecture of the SEJAM2 multi-domain simulator with tight coupling of physical and computational simulation of sensor networks*
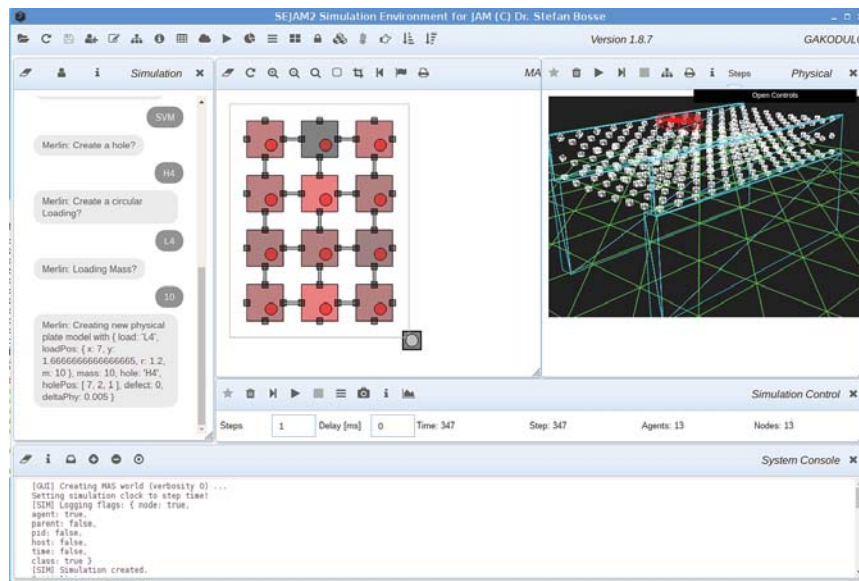


*Figure 2. SEJAM2 software screenshot*

## II.3  Synthetic Sensors

The physical MBP simulation is primarily used to compute sensor data passed to the digital sensor network. There are basically two classes of sensors and measuring techniques used in SHM and NDT:

1. Strain sensors applied to the surface or integrated in the surface layer of a DUT

2. Ultrasonic acoustic sensors and actuators coupled to the surface of the DUT (active measuring technique), or more generally acoustic sensors detecting vibrations of the DUT (passive measuring technique).

Sensor data of the first class can be directly calculated from the mass-spring network requiring only the distances between mass nodes (available directly from the *CANNON* engine). A low mass-node density is still sufficient. The second class requires the simulation of the propagation of elastic and acoustic (e.g., lamb) waves in the material, which requires a high density of mass-nodes. Fig. 3 shows signals of a spatially distributed strain-gauge sensor network attached to the surface of rectangular plate and getting time-resolved sensor data from the MBP simulation. These plots show the fine-grained and highly time-resolved  dynamic behaviour of the plate (swinging, starting with an initial and terminating with a final shape caused by gravity).
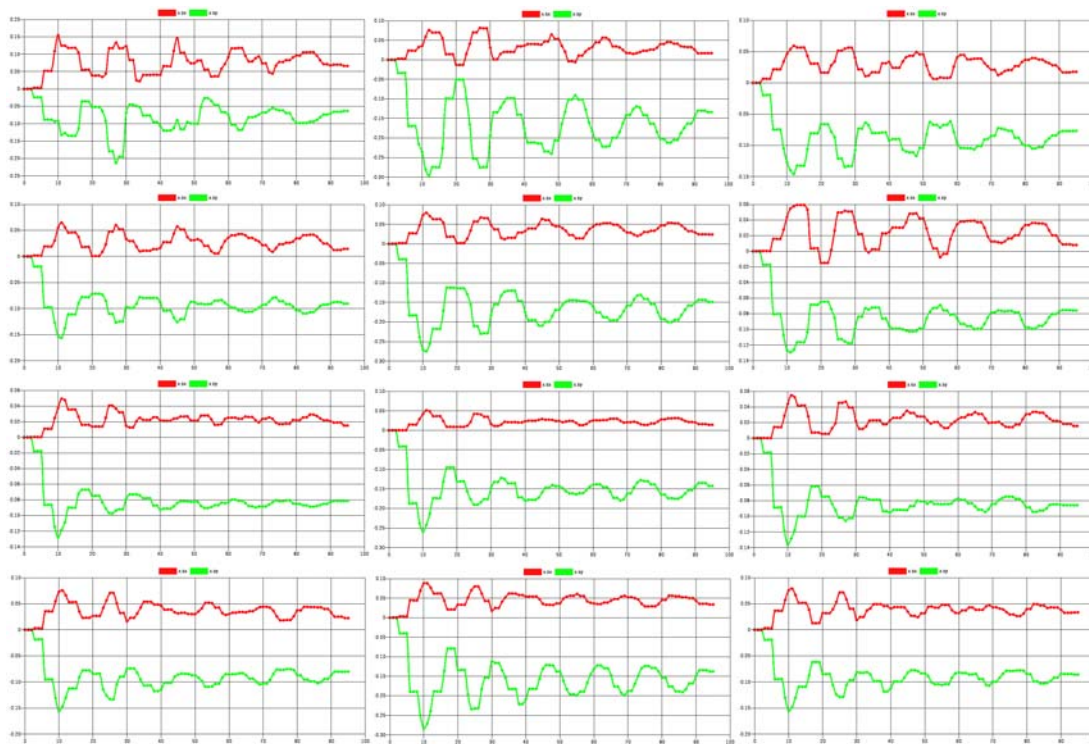


*Figure 3. Synthetic strain-gauge sensors in a 3x4 network (spatially distributed over a plate DUT surface, and at each position two perpendicular orientated sensors along x- and y-axis) with dynamic time-dependent structure behaviour. There was an hidden hole inside the structure near by the left upper corner. (x-axis: time in simulation steps, y-axis: sensor signal in arbitrary units). Note: y-scales differ in the single plots.*

## III.  Machine Learning

Machine learning consists basically of three functions:

1. The learned model $M(x)$ mapping an input vector $x$ (sensor data) on an output vector $y$ (prediction of system state)

2. The training function *learn* deriving the model function $M$ from (known and labelled) training data

3. The prediction function *apply* applying the model function $M$ to unknown (unlabelled) sample data

Learning and prediction using sensor data can be performed in two dimensions (see Fig. 4):

**Spatial domain**. The sensor data $D(x, t_0)$ consists of data from spatially distributed sensors (either the entire sensor network or a sub-domain) sampled at a specific time point $t_0$ (or accumulated over a time period).

**Time domain**. The sensor data is time dependent $d(t)$ and time series of single or a set of sensors are recorded and evaluated.
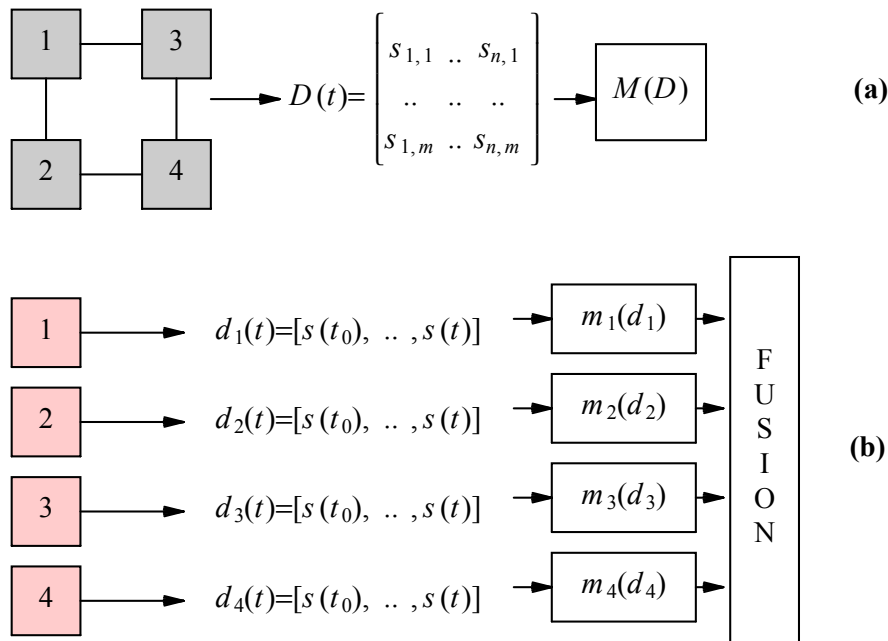


*Figure 4. (Left) Spatial (a) and temporal (b) sensor data used for learning (Right) Single-instance centralised (a) and multi-instance decentralised (b) learning with fusion (consensus solving)*

$$d_t(t) = \{s(t_0), s(t_1), s(t_n), .., s(t)\}$$

$$D_s(x, t_0) = \begin{pmatrix} s_{1,1}(t_0) & \cdots & s_{n,1}(t_0) \\ \vdots & \ddots & \vdots \\ s_{1,m}(t_0) & \cdots & s_{n,m}(t_0) \end{pmatrix} \tag{2}$$

$$D_{t-s}(x, t) = \left\{ \begin{pmatrix} s_{1,1}(t_0) & \cdots & s_{n,1}(t_0) \\ \vdots & \ddots & \vdots \\ s_{1,m}(t_0) & \cdots & s_{n,m}(t_0) \end{pmatrix}, .., \begin{pmatrix} s_{1,1}(t) & \cdots & s_{n,1}(t) \\ \vdots & \ddots & \vdots \\ s_{1,m}(t) & \cdots & s_{n,m}(t) \end{pmatrix} \right\}$$

Finally, learning and prediction can be performed by a single instance using spatially global sensor data or by multiple distributed instances (e.g., applied to temporal data record). Multiple learner instances create multiple prediction models $m_i$ that must be fusioned to compute a global prediction.

## IV. Decision Tree Learner

### IV.1 Training Sets

The original *ID3* algorithm by J. R. Quinlan [16] is an iterative algorithm for constructing Decision Trees (DT) from a training data set **D**.

**D** is a table with columns $(x_1, x_2, .., x_n, y)$ and a number of rows. Each table cell has a value $v \in V(x)$ (of attribute variable $x$) and $t \in T$ for the target attribute variable. Each column $c(x_i)$ of the variable $x_i$ has a set of values $\{c_v = v_{i,j} : j = \{1, 2, .., m\}\}$, with $m$ as row number of the data table.

| $x_1$ | $x_2$ | .. | $x_n$ | $y$ |
|---|---|---|---|---|
| $v_{1,1}$ | $v_{2,1}$ | .. | $v_{n,1}$ | $t_1$ |
| .. | .. | .. | .. | .. |
| $v_{1,m}$ | $v_{2,m}$ | .. | $v_{n,m}$ | $t_m$ |

*Table 1. Training data table format*

The main difference between the *ID3* and *C45* learner and models is related to the data type of the input variables *x*. *ID3* only supports sets of discrete values or symbols (categorical data), whereas *C45* supports both numerical and categorical data. In case of numerical data, *C45* constructs binary trees with relational edges. Categorical data (variables) produce n-ary trees with edges representing discrete values of the node vari-

able.

## IV.2  Entropy

Consider a column of the table, e.g., the target attribute column of $y$, $c(y)$. There is a finite set of unique values $V=\{v_1,v_2,..,v_u\}$ that any column $c(x)$ (and $c(y)$) can hold. Now it is assumed that some values occur multiple times. The information entropy, i.e., a measure of disorder of the data, of this (or any other) column $c$ (of variables $x/y$) is defined by the entropy of the value distribution *entropyN*:

$$entropy_N(N) = \sum_{i=1}^{n} -p_i\log_2 p_i, \text{with } p_i = \frac{N_i}{\sum N}$$

$$entropy(c) = \sum_{v \in V(c)} -p_v\log_2 p_v, \text{with } p_v = \frac{|c_v|}{|c|} \tag{3}$$

In general, the information entropy of the value distribution of a column $c(x_i)$ related to the outcome of the target variable $Y$ is given by:

$$Entropy(T,c) = \sum_{v \in V(c)} p_v entropy_N(\{|c_v(t)| : t \in T\}),$$

$$\text{with } p_v = \frac{|c_v|}{|c|} \text{ and} \tag{4}$$

$$\{|c_v(t)| : t \in T\} = \{|c_v \text{ with } y = t_1|, |c_v \text{ with } y = t_2|, ..\}, t_i \in T$$

with $v \in V(c)$ as the possible unique values of the attribute variable $x$ and $T$ as the values of the target attribute.

The ID3 algorithm now starts with an empty tree and the full set of attribute variables $A=\{x_1,..,x_n\}$ and the full data set $D$. The entropy for each column is calculated (applying Equations 4 and 5) and finally the information counting gain for each column with respect to the target attribute distribution $T$ in this column:

$$Gain(T,c) = entropy(T) - Entropy(T,c) \tag{5}$$

The column $c(x_i)$ with the highest gain associated with attribute variable $x_i$ is selected for the first tree node splitting and is removed from the set $A$. For each value of the attribute occurring in the selected column a new branch of the tree is created (i.e., each branch contains the rows that have one of the values of the selected attribute). In the next iteration a new attribute (column) is selected from the remaining attribute set until there are no more attributes. A zero gain indicates a leave (i.e., all rows select the same target attribute, i.e., $T=\{t\}$).

# V.  ICE Decision Tree Learner

### V.1  Noise and Value Intervals

The ID3 and C45 learning algorithms were designed with categorical data and always distinguishable numerical data in mind [16]. Two numbers $i$ and $j$ are always distinguishable if $i \neq j$, i.e., they are always different independent how close together the values are. However, real-world data is noisy, and two numbers can only be distinguished if they are separated at least by a distance of $\varepsilon$, i.e., they are only considered as different feature values if the noise margin is lower than their distance. The problem of ambiguous data values is relevant for all DT learners.

For this reason, a hybrid *ID3-C45* decision learner algorithm extending variables with $\varepsilon$-intervals was created (Interval Column Entropy, *ICE*). The new algorithm is compared with other algorithms in Sec. VIII. Each data variable $x_i$ is assigned an $\varepsilon_i$ value (individually) that is used to transform column values to $2\varepsilon$ value intervals, i.e., $[v_x-\varepsilon_i, v_x+\varepsilon_i]$. Now, the previous entropy and gain computations are performed with $\varepsilon$-variables and interval arithmetic.

| $x_1 \pm \varepsilon_1$ | $x_2 \pm \varepsilon_2$ | .. | $x_n \pm \varepsilon_n$ | $y$ |
|---|---|---|---|---|
| $v_{1,1} \pm \varepsilon_1$ | $v_{2,1} \pm \varepsilon_2$ | .. | $v_{n,1} \pm \varepsilon_n$ | $t_1$ |
| .. | .. | .. | .. | .. |
| $v_{1,m} \pm \varepsilon_1$ | $v_{2,m} \pm \varepsilon_2$ | .. | $v_{n,m} \pm \varepsilon_n$ | $t_m$ |

*Table 2. Extending data variables with $\varepsilon$ value intervals; Only non-overlapping intervals contribute to the set of unique values $V_\varepsilon \subset V$*

### V.2  Gain Computation

The following *gain* computation is performed for each column of the data training table, shown in Tab. 2 using interval arithmetic. Instead counting all different values in a column creating the set **V**, only non-overlapping $2\varepsilon$-values are counted as unique

values creating the sub-set $\mathbf{V}_\varepsilon \subset \mathbf{V}$.

$$Gain_\varepsilon(T, c, \varepsilon) = entropy(T, \varepsilon) - Entropy_\varepsilon(T, c, \varepsilon)$$

$$Entropy_\varepsilon(T, c, \varepsilon) = \sum_{v \in V_\varepsilon(c)} p_v entropy_N(\{|c_v(t)| : t \in T\})$$

$$V_\varepsilon = \{c_i : [v_i - \varepsilon, v_i + \varepsilon] \cap [v_j - \varepsilon, v_j + \varepsilon] = \emptyset, \forall i \neq j, c_i \in c, c_j \in c\}$$

(6)

Instead using relational splitting as in the binary trees created by the C45 algorithm (i.e., $\{n_1|x_i<v, n_2|x_i \geq v\}$), the *ICE* algorithm creates n-ary trees with child nodes $n_i$ providing interval value splitting points ($\{n_1|x_i \in [v_1-\varepsilon_1, v_1+\varepsilon_1],..\}$), similar to the *ID3* discrete categorical value splits. Each split interval is computed from column interval values from all rows with the same target variable value (all rows with the same target variable value create a cluster).

A nearest-neighbour approach is used to find the best matching child node on prediction. Either a variable value is contained in one of the possible split child node intervals (preferred non-overlapping), or the child node with nearest distance to its value interval is chosen.

The main advantage of the new *ICE* algorithm compared to traditional decision tree learners is the improved gain computation for the selection of suitable and strong feature variables and tree splitting. The entropy and gain of a feature variable column of the training data table depends on the number of unique value sets in this column. Without noise consideration, different values (independent of their distance from each other) lead to a high number of unique values. With consideration of noise and $\varepsilon$ value-intervals, the number of unique values in a column can decrease significantly, separating strong and weak feature variable columns (with respect to the split selection).

## VI. Comparison of Decision Tree Models



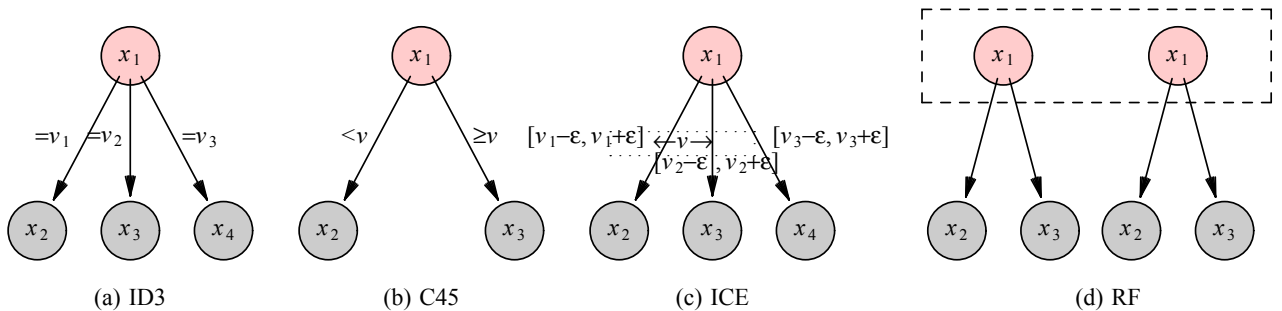(a) ID3     (b) C45     (c) ICE     (d) RF

*Figure 5. (a) Categorical Data Tree (b) Numerical Relational Data Tree (c) Numerical Interval Tree with nearest-neighbour approximation (d) Random Forest trees*

## VII.  Global vs. local Learning

Global learning collects spatially distributed sensor data and processes the entire data with one learning instance. In contrast, distributed local learning processes the local sensor data (of a node or a spatially bounded region of nodes). This learning architecture introduces multiple learning instances, requiring a global consensus algorithm upon prediction to decide one global decision. A simple type of such consensus algorithm is majority voting.

Global learning can use snapshots (at a specific time) or time-accumulated sensor data to avoid a large amount of data variables, whereas local learning can process time-resolved data, too, without exceeding computational complexity that can be handled, e.g., in real-time.

## VIII.  Experiments and Evaluation

Experiments were performed using the *SEJAM2* simulation environment. A rectangular plate was used as a typical Device under Test (DUT). Two sides of the plate were fixed by two walls. The DUT was modelled with the MBP models and a grid size of $14 \times 8 \times 3$ mass nodes connected with springs (elastic model), shown in Fig. 6 (a). Bending by gravity was used a typical load situation. Starting from an initial state of the DUT, the mass nodes are moved towards the gravity force direction resulting in a typical bending structure.

The sensor network consists of $3 \times 4$ sensor nodes, shown in Fig. 6 (b). Each node samples two connected synthetic strain-gauge sensors (orthogonal orientated), shown in Fig. 6 (c). The originally undamaged plate DUT can be modified by adding holes inside (by removing mass nodes of the DUT) and prediction can be disturbed by applying additional load to the upper surface, shown in Fig. 6 (d).
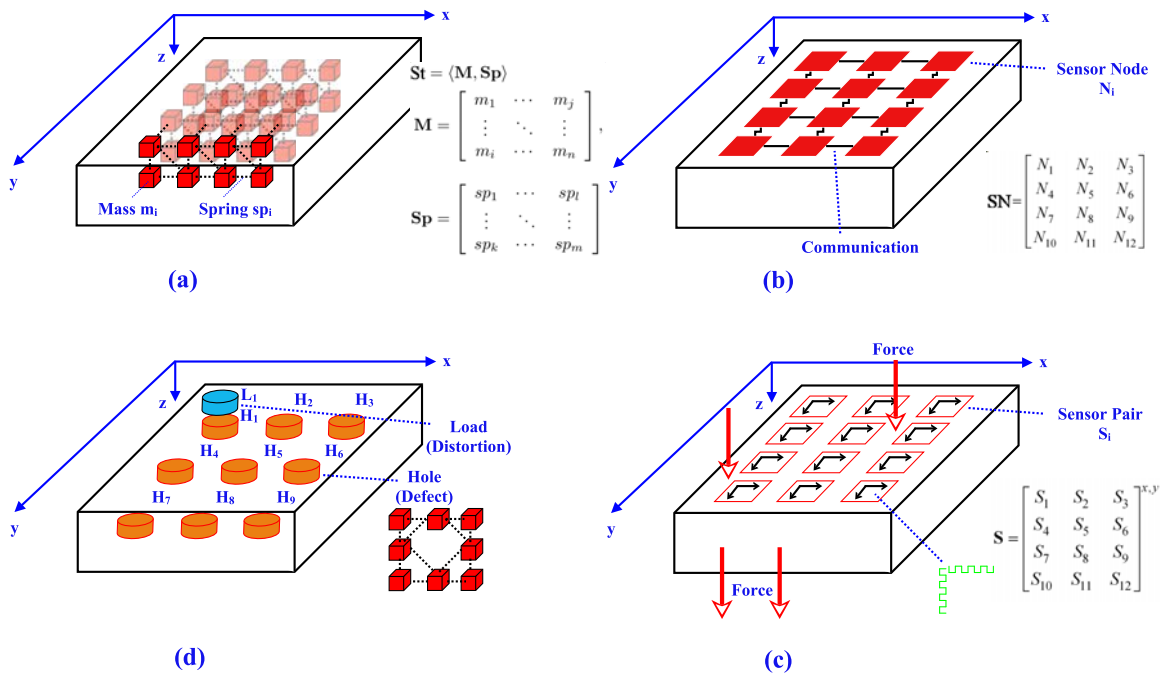
*Figure 6. (a) MBP Modell of a plate (DUT) (b) Sensor Network applied to surface of DUT (c) Strain-gauge Sensors connected with sensor nodes (d) Hidden  holes in the DUT (red) and additional load applied to the surface (blue)*

The following learning algorithms and models were used:

- Classical decision tree learner (*C45*)

- Advanced decision tree learner with interval arithmetic and nearest-neighbour approximation (*ICE*)

- Random forest tree learner (*RF*)

- Single layer perceptrons (one layered artificial neural network, *SLP*)

- Multi layer perceptrons (deep learning with hidden layers, *MLP*)

- Multi-label Support Vector Machines (*SVM*)

Two different learning domain strategies were investigated:

- Global learning with one learner instance (see Fig. 4 a) using a sensor snapshot (after the DUT dynamics is below a threshold)

- Local learning with 12 node-based learner instances and global fusion (see Fig. 4 b) using time records of the sensor signals (starting with the begin of DUT dynamics)

### VIII.1  Global Learning

With 12 sensor nodes and each sensor node connected with a pair of strain-gauge sensors, there are 24 input variables. The neural networks consist of 24 input neurons (12 sensor pair feature variables) and 10 output neurons (nine damage locations and the undamaged case). The multi-label *SVM* consists of 10 parallel binary classifier *SVM*s (one for each damage feature).

| ML | Parameter | Learning Time | Modelsize (Bytes) |
|---|---|---|---|
| C45 | - | 8s | 4k |
| ICE | $\varepsilon$=0.01 | 100ms | 16k |
| SLP | *iter*=1000 | 1s | 190k |
| MLP[1] | *iter*=1000, $layers_{hidden}$ = [5] | 2s | 210k |
| MLP[2] | *iter*=20000, $layers_{hidden}$ = [5] | 22s | 210k |
| SVM | *iter*=1000, *kernel*={*type*: *rbf*, *C*:0.5, $\sigma$:0.1} | 90s | 260k |
| RF | $depth_{max}$=10, *trees*=5 | 150ms | 1.2M |

*Table 3. Comparison of different learned models (200 data sets of all sensors; global learning) showing learning time and model data size.*

The various  ML algorithms differ in learning time and model data size, shown in Tab. 3 for 200 training data sets. The learners requires accurate setting of a parameter set (except the *C45* learner). The neural networks require the specification of the model architecture (number of hidden layers, number of neurons, and the neuron interconnect graph), whereas the other model architectures are automatically determined by the learner (but still influenced  by the learning parameters).

The *ICE* algorithm has the fastest learning time in the milliseconds scale, followed by the random forest learner. The neural network learners require much higher learning times in order of magnitude of seconds. Adding hidden layers (here only one hidden layer with five neurons) requires a significant higher amount of learning iterations (about 10-20 times) to get reasonable prediction results. The *SLP* can be trained with less than 1000 iterations and still results in a high prediction accuracy about 80-98% (see Fig. 7), whereas a *MLP* predicts only noise at 1000 iterations. But the *MLP* out-

performs the *SLP* if a high training iteration count greater than 10000 iterations is used, with the disadvantage of high learning times (up to 100 seconds for 200 training sets). The slowest algorithm in comparison is *SVM* as result of the binary classifier nature of *SVM*s. To provide multi-label classification, an *SVM* is required for the prediction of each label (i.e., here 9 damage locations and the undamaged case label). Although the random forest can compete with the new *ICE* learner in learning time, the model size is the largest of all compared models and the prediction results are on the lower bound in this comparison.
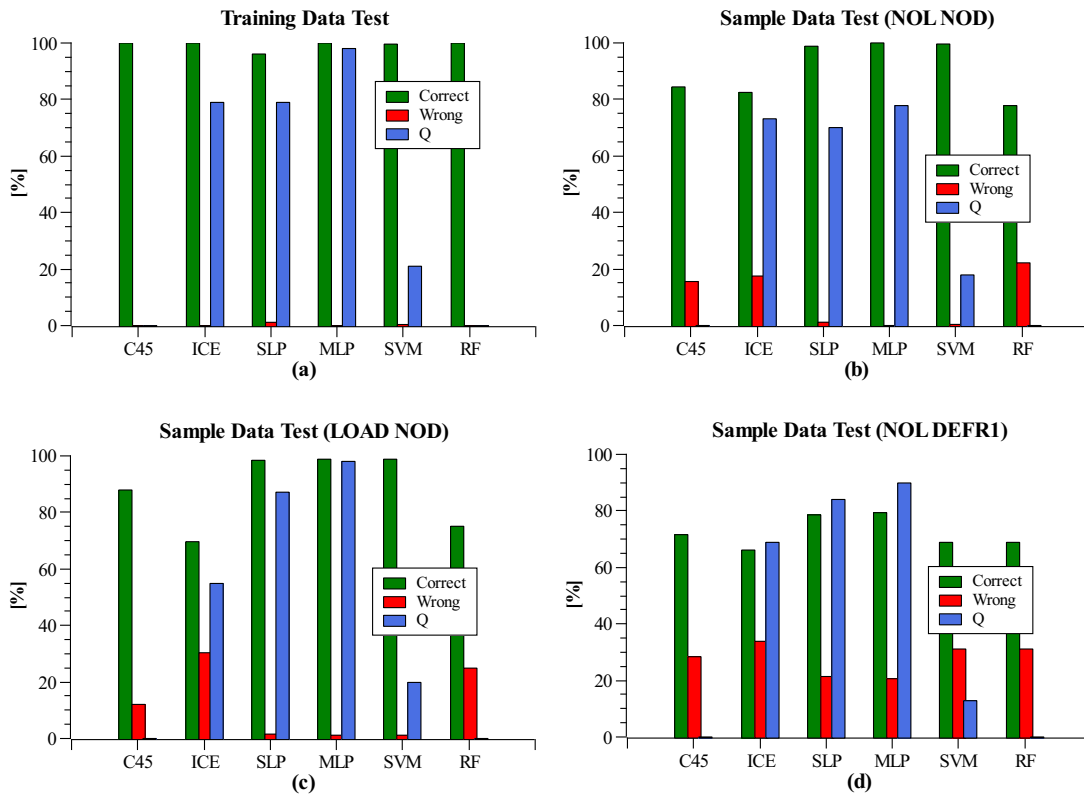


*Figure 7. Simulation results and comparison of different ML algorithms for global learning (a) Test data used for training (b) Sample data (c) Sample data with additional load distortion (d) Sample data with random sensor defect*

The computation of the quality confidence marker *Q* depends in the learned model and algorithm. For neural networks, the output value of the most significant firing output neuron is used (range [0,1). *SVM*s usually uses a threshold function to output a binary set of values (e.g., [-1,1). The output of the *SVM* before applying the threshold function can be used an approximation of the *Q* marker, although without no strict and fixed bounds. The classical C45 decision tree and the random forest trees do not deliver any suitable *Q* marker. In contrast to C45/ID3, the *ICE* predictor uses nearest neighborhood estimation to find the best matching path in the decision tree. The dis-

tance from each node variable value to its nearest child node value is used as $Q$ marker (accumulated over all nodes along a tree search path).

The evaluation results shows that the $Q$ confidence marker is not always suitable to give a measure of trust. There is no strong correlation between the $Q$ value and the correctness probability in case of the *ICE* learner. The *MLP* results show similar $Q$ values (80-90%) for training and sample data, but the failure rate in the last situation (defect sensors) is significantly increased. The *SVM* values for $Q$ are always low (indeed using a best-winner approach selecting the *SVM* classifier with the highest output but still negative value!).

## VIII.2  Local Learning

In contrast to the previously evaluated global learning approach using sensor snapshots of all spatially distributed sensors at a specific time, the local learning approach uses time-resolved records of the sensor signals with a given capture window (32 samples). Furthermore, each sensor node implements a single learner instance learning local models that are applied to local sensor data only. Therefore, the input data vector $X$ consists of 64 variables.

There are only two target labels for each learning instance that have to be classified: (DAMAGE) meaning a damage was detected within a region around the sensor node (radius of 1.5 sensor distance lengths) and (NODAMAGE) meaning no damage within this region was detected. In the evaluation, the number of "No damage" cases for each node is much higher than the number of "Damage near by" cases (naturally).

The evaluation of the local learning approach with nine different damage locations and an unmodified structure is shown in Fig. 8. Again, training data tests and sample prediction without and with disturbance (additional loads, defect sensors randomly chosen) is shown. Different quality parameters were retrieved from the analysis. The first pair *correct*/*wrong* tests each single node whether the damage within the neighbouring region was correctly found or not. The second pair *gcorrect*/*gwrong* uses global fusion by computing the average position of all sensor nodes detecting a damage. If the average position is near by the real damage location (within a radius of 1.5 node distance units), the classification is counted as correct, otherwise as wrong.
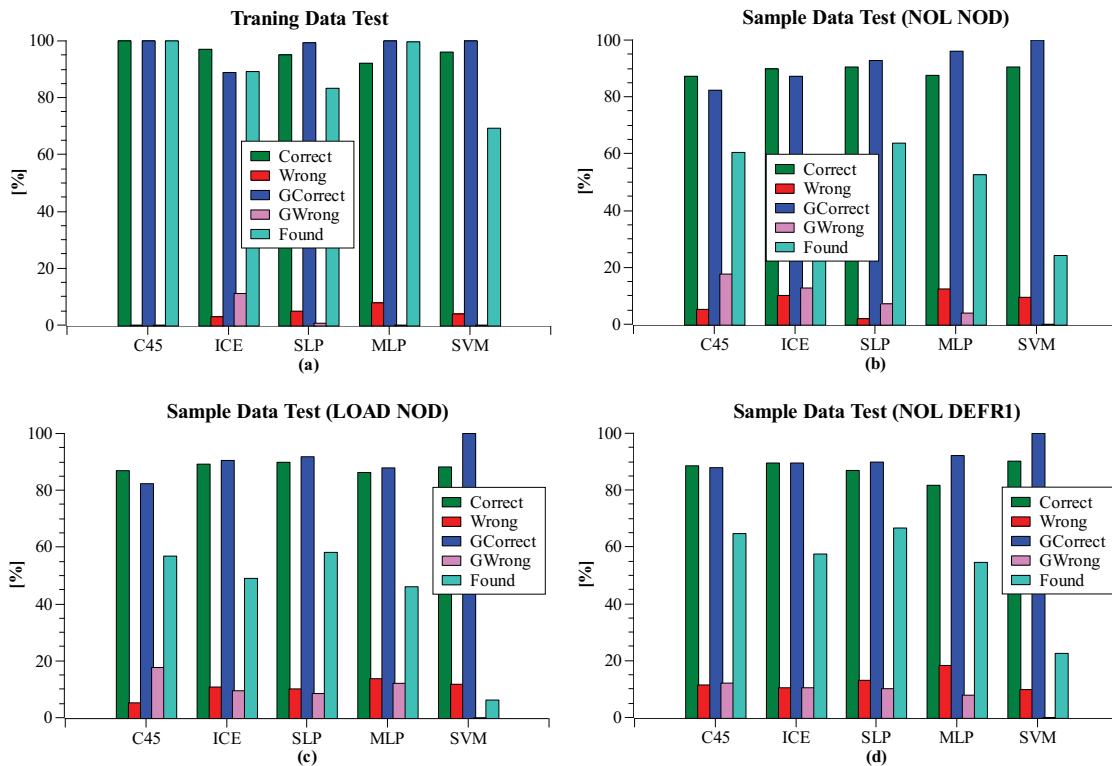
*Figure 8. Simulation results and comparison of different ML algorithms for local learning (a) Test data used for training (b) Sample data (c) Sample data with additional load distortion (d) Sample data with random sensor defect*

All learning algorithms show a high correct-positive and correct-negative single-node prediction probability with zero or only a few wrong-positive and wrong-negative predictions. But remember that the NODAMAGE feature has a 10 times higher weight with respect to each single node. The global fusioned damage prediction quality (with equally distributed weights of the ten different damage features) show the best result for the *SVM* learner, although the single local DAMAGE hit rate is rather low compared with the other learners. In contrast to the global learner, the *MLP* model shows lower prediction quality than the *SLP*. The decision tree learner can still compete with the complexer neural networks and *SVM*, leading to a prediction accuracy higher than 80%.

### VIII.3  Efficiency Comparison

The efficiency of a learner is defined by:

$$\epsilon = \frac{p}{LD} \tag{7}$$

where $p$ is the prediction accuracy in %, $L$ is the learning time in seconds, and $D$ is the model data size in kB. In the following Tab. 4 the efficiencies of the different ML algorithms are compared using the results from the previous sections (global learner instance). The prediction accuracy is an average value of all four test cases (training data, sample data, sample data with additional loads, and sample date with random defect sensors).

| C45 | ICE | SLP | MLP | SVM | RF |
|-----|-----|-----|-----|-----|-----|
| 3 | 50 | 0.5 | 0.02 | 0.004 | 0.4 |

*Table 4. Comparison of efficiencies for different ML algorithms (global learning instance).*

## IX.  Conclusion

A multi-domain simulation framework realizing tight coupling of physical simulation of mechanical structures and computational simulation of sensor networks was used to investigate different ML approaches and algorithms used for the prediction of hidden damages. The main focus was the deployment of low-cost non-calibrated strain-gauge sensors. It could be shown that simple decision tree models are generally suitable for damage prediction. A new advanced decision tree learner *ICE*  was introduced. This learner takes noise of sensor data into consideration leading to improved models and prediction accuracy. Additionally, this new learner outperforms classical decision tree learners and neural networks regarding learning time (in milliseconds) and model data size. The comparison of single and multi-layer neural networks (deep learning) poses no significant advantage over multi-layer networks with respect to prediction accuracy. All learners can be applied in the sensor spatial and time-domain, and in centralised single-instance and multiple-instance decentralised learning architectures. Although *SVM*s require the highest learning time, they outperform all other algorithms in multiple-instance decentralised learning architectures using time records of sensor signals.

## X. References

1.   Supreet, A. K., Harley,  J., *Structural Damage Detection Using Deep Learning of Ultrasonic Guided Waves*, in AIP Conference Proceedings, 2017.

2.   Bosse, S. *Industrial Agents and Distributed Agent-based Learning*, 3rd International Electronic Conference on Sensors and Applications . 15-30 Nov. 2016, MDPI, 2016, DOI:10.3390/ecsa-3-S2004.

3.   Miersch, N., Roßmann, R., Holz, C., *Grundlagenuntersuchung zu ausgewählten finiten Elementen der Strukturmechanik für ein einfaches validierbares FE-Modell*, WISSENSCHAFTLICHE BEITRÄGE, TH Wildau, vol. 21, pp. 61-70, 2017

4.   Mucha, W., *Real-time finite element simulations on ARM microcontroller*, Journal of Applied Mathematics and Computational Mechanics, vol. 16, no. 1, pp. 109-116, 2017.

5.   Rahnejat, H. Mult-body dynamics: Historical evolution and application. Proceedings of the institution of Mechanical Engineers 214 (1999) 149-173.

6.   Sousa, L., Verissimo, P., Ambrosio, J. Development of generic multibody road vehicle models for crashworthiness. Multibody System Dynamics 19 (2008) 133–158.

7.   Ambrosio, J., Quental, C., Pilarczyk, B., Folgado, J., Monteiro, J.  Multibody biomechanical models of the upperlimb. Procedia IUTAM 2 (2011) 4-17.

8.   Lee, S.-H., Kim, J., Park, F. C., Kim, M., Bobrow, J. E. Newton-Type Algorithms for Dynamics-Based Robot Movement Optimization. IEEE Transactions on Robotics 21 (2005) 657-667.

9.   Schiehlen, W. Multibody System Dynamics: Roots and Perspectives. Multibody System Dynamics 1 (1997) 149–188.

10.   Yoo, W.-S., Kim, K.-N., Kim, H.-W., Sohn, J.-H. Developments of multibody system dynamics: computer simulations and experiments. Multibody System Dynamics 18 (2007) 35–58.

11.   Zarate, F., Onate, E.A simple FEM–DEM technique for fracture prediction in materials and structures. Comp. Part. Mech. 2 (2015) 301–314.

12.   Raymond, S. J., Jones, B., Williams, J. R. A strategy to couple the material point method (MPM) and smoothed particle hydrodynamics (SPH) computational techniques. Comp. Part. Mech. 5 (2018) 49–58.

13.   Hedman, S., CANNON, http://schteppe.github.io/cannon.js, retrieved on 1.11.2019

14.   Bosse, S. Lehmhus, D. , *Material-integrated cluster computing in self-adaptive robotic materials using mobile multi-agent systems*, Cluster Computing, doi 10.1007/s10586-018-02894-x, Volume 22, Number 3, pp. 1017-1037, 2019 ISSN 1386-7857

15.     Bosse, S., Engel, U., *Real-time Human-in-the-loop Simulation with Mobile Agents, Chat Bots, and Crowd Sensing for Smart Cities*, Sensors (MDPI), 2019, doi: 10.3390/s19204356

16.     HSSINA, B. , MERBOUHA, A. , EZZIKOURI, H. , ERRITALI, M., *A comparative study of decision tree ID3 and C4.5*, (IJACSA) International Journal of Advanced Computer Science and Applications, Special Issue on Advances in Vehicular Ad Hoc Networking and Applications, 2014.